Ultraviolet Cavity Ringdown Spectra and the $S_1(n,\pi^*)$ Ring-Inversion Potential Energy Function for 2-Cyclohexen-1-one-d_0 and Its 2,6,6-d_3 Isotopomer

Mohamed Z. M. Rishard,[†] Elizabeth A. Brown,[‡] Logan K. Ausman,[‡] Stephen Drucker,*[,‡] Jaebum Choo,[§] and Jaan Laane*[,†]

Department of Chemistry, Texas A&M University, College Station, TX 77843-3255, Department of Chemistry, University of Wisconsin—Eau Claire, Eau Claire, Wisconsin 54702-4004, and Department of Chemistry, Hanyang University, Ansan 425-791, Korea

Received: July 6, 2007; In Final Form: October 8, 2007

The cavity ringdown spectra of 2-cyclohexen-1-one (2CHO) and its 2,6,6-d_3 isotopomer (2CHO-d_3) have been recorded in the spectral region near their $S_1(n,\pi^*)\leftarrow S_0$ band origins which are at 26 081.3 and 26 075.3 cm^{-1}, respectively. The data allow several of the quantum states of ν_{39}, the ring inversion, to be determined for both the ground and excited electronic states. These were utilized to calculate the one-dimensional potential energy functions which best fit the data. The barriers to inversion for the S_0 and $S_1(n,\pi^*)$ states were found to be 1900 ± 300 and 3550 ± 500 cm^{-1}, respectively. Density functional theory calculations predict values of 2090 and 2265 cm^{-1}, respectively.

Introduction

The photochemistry of conjugated cyclic enone molecules has been investigated from a mechanistic perspective for several decades.[1] Computational investigations in this area have been particularly active, including studies of cycloaddition reactions[2] as well as Type B,[3] lumiketone,[3] and Type C[4] rearrangements. These studies, along with supporting experimental evidence, show that photoexcitation of the conjugated enone initially prepares the $S_1(n,\pi^*)$ state. This is followed by nonradiative decay (intersystem crossing) along a pathway that includes the lowest energy $T(n,\pi^*)$ or $T(\pi,\pi^*)$ triplet potential-energy surface (or both). The triplet states are relatively long-lived and reactive.

The mechanism and outcome of these photoreactions depend on the detailed topologies of the excited-state potential energy surfaces. A key feature is the energetic accessibility of the various triplet electron configurations and conformations. The mechanism also depends on specific nonradiative decay paths, both from the initially prepared $S_1(n,\pi^*)$ to the triplet state(s), as well as from the triplet excited states to the ground-state surface of the product. Computational studies of cyclic enone photochemistry have focused on determining such details accurately.

These computational initiatives are supported by spectroscopic studies of the excited states. Vibronically resolved spectra provide a rigorous test of computed potential energy surfaces, via comparison of experimental vs calculated vibrational frequencies, electronic excitation energies, and geometry changes associated with electronic excitation.

In previous spectroscopic work from our laboratories we focused on 2-cyclopenten-1-one (2CPO), one of the simplest conjugated cyclic enones. We determined an experimental potential-energy function for the ring-bending vibrational mode in the S_0 ground electronic state,[5] as well as in the $S_1(n,\pi^*)$ [6] and $T_1(n,\pi^*)$ [7] excited states. The minimum in the ring-bending function is at a planar geometry in the S_0 state. The $S_1(n,\pi^*)$ state was also found to be planar but less rigid than the ground state. The $T_1(n,\pi^*)$ state is slightly puckered, with a small (43 cm^{-1}) barrier to planarity. The tendency toward planarity in 2CPO has been invoked[8] to explain the relatively long transient absorption lifetime[9] measured for its lowest triplet state in solution.

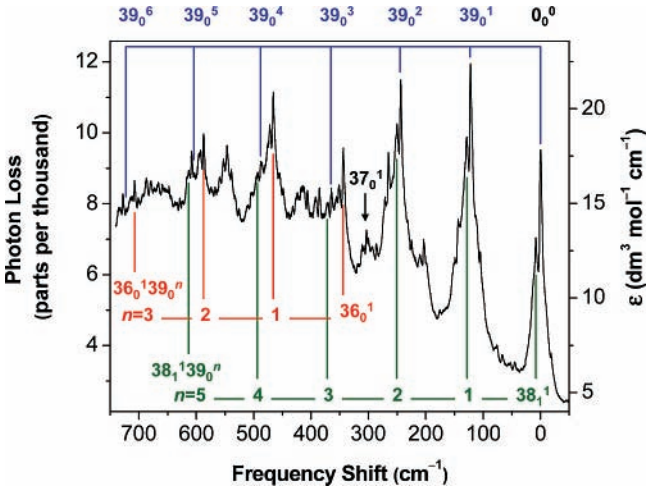

Figure 1. CRD spectrum of 2CHO vapor at room temperature. The pressure in the sample cell was 13 Pa (0.1 Torr). This spectrum is a composite of several scans recorded over adjacent wavelength regions near the $S_1(n,\pi^*) \leftarrow S_0$ origin. Frequencies are relative to the 0_0^0 band at 26 081.3 cm^{-1}. Colored tie lines attached to an assigned origin indicate a progression in the excited-state inversion mode (ν_{39}).

The homologous 2CHO molecule has a larger ring and favors a nonplanar geometry to minimize the angle strain. Previously published far-infrared spectra[10] show that the 2CHO molecule has a nonplanar equilibrium geometry in its S_0 state. In 2004 we used ultraviolet cavity ringdown (CRD) spectroscopy to record the $S_1(n,\pi^*)\leftarrow S_0$ electronic band system of 2CHO.[11] From the vibronic hot bands ($v'' > 0$) in the CRD spectrum,

[†] Texas A&M University.
[‡] University of Wisconsin—Eau Claire.
[§] Hanyang University.

10.1021/jp075281c CCC: $40.75
Published on Web 12/15/2007

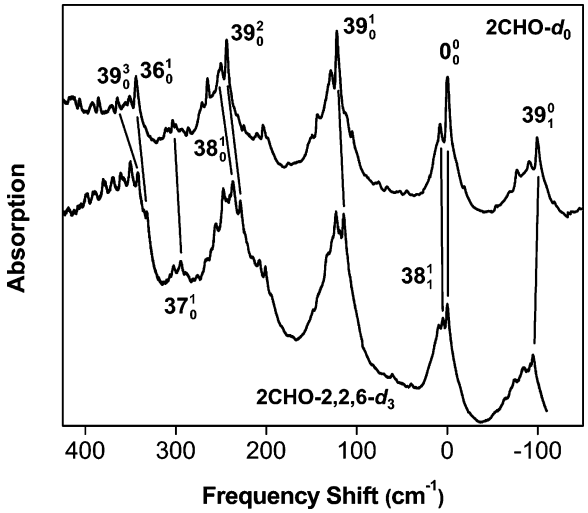

Figure 2. Comparison of CRD spectra for CHO-d_0 and CHO-d_3. Frequencies are relative to the respective $S_1 \leftarrow S_0$ band origins, 26 081.3 cm^{-1} for CHO-d_0 and 26 075.3 cm^{-1} for CHO-d_3.

combined with the previous far-infrared spectral data,[10] we determined the one-dimensional ring-inversion potential energy function for the S_0 state. The barrier to planarity was found to be 1900 ± 300 cm^{-1}, consistent with the calculated value of 2090 cm^{-1} by density functional theory (DFT) using the B3LYP/6-311+G(d,p) basis set.[11]

In the electronic excited states of 2CHO the conjugation is disrupted, leading to an expectation of even more ring flexibility than in the ground state. Computational studies of the 2CHO triplet states show that the $T_1(\pi,\pi^*)$ state has a twisted equilibrium geometry that facilitates a rapid intersystem crossing to highly excited vibrational levels of S_0.[8] The nonradiative decay sequence $S_1(n,\pi^*) \rightarrow T_2(n,\pi^*) \rightarrow T_1(\pi,\pi^*) \rightarrow S_0$ has been proposed[8] to explain the short triplet-state lifetime of 2CHO observed[9] following photoexcitation of the S_1 state. The S_1 state of 2CHO also has nearly zero quantum yield for fluorescence,[12] another observation attributable to the nonradiative decay sequence. By contrast, the fluorescence quantum yield in the more rigid 2CPO molecule is significant and has permitted extensive characterization of its S_1 state via fluorescence excitation spectroscopy.[6]

In this paper we characterize the $S_1(n,\pi^*)$ state of 2CHO by analyzing the $S_1(n,\pi^*) \leftarrow S_0$ vibronic band system observed in the CRD spectrum. CRD spectroscopy,[13] rather than fluorescence excitation, was chosen for the experiment because CRD is based on absorption and is therefore amenable to molecules such as CHO that are subject to rapid nonradiative decay processes. Moreover, the $\pi^* \leftarrow$ n transitions of ketones and enones are orbitally forbidden and hence typically several orders of magnitude weaker than fully allowed $\pi^* \leftarrow \pi$ transitions. The high sensitivity of the CRD technique permits observation of the weak $\pi^* \leftarrow$ n transitions readily.

In our previous work[11] we also presented in part the ring-inversion transitions in the $S_1(n,\pi^*) \leftarrow S_0$ CRD spectrum, but the potential energy function for the S_1 state was not determined. In the present paper we report additional CRD data for 2CHO as well as its 2,6,6-d_3 isotopomer. We have analyzed these data to determine the ring-inversion potential energy function for the S_1 state. We expected (and observed) a higher barrier to planarity than in the ground state because of the disruption of conjugation in the S_1 state. The experimental results will also be compared to the results from DFT calculations.

TABLE 1: CRD Transition Frequencies[a] (cm^{-1}) and Assignments for 2CHO

observed	inferred[b]	calculated[c]	assignment	
−303.2	−303.2	308	37_1^0	
−294.8	−293.9 [d]		39_3^0	
−243.0	−243.8	241	38_1^0	251.9 − 8.1
−197.0	−197.0		39_2^0	
−191.7	−190.5		$38_1^1 39_2^0$	251.9 − 442.2
−99.2	−99.0 [e]	103	39_1^0	
−90.5	−91.7		$38_1^1 39_1^0$	251.9 − 343.6
−76.9	−74.9		39_2^1	122.1 − 197.0
8.1	8.1		38_1^1	251.9 − 243.8
29.0	29.0		$38_1^1 39_1^1$	372.6 − 343.6
44.9	46.8		39_2^2	243.8 − 197.0
52.5	50.6		$38_1^1 39_2^2$	492.8 − 442.2
55.9 sh	54.9		$38_0^1 39_2^0$	251.9 − 197.0
122.1	122.1	121	39_0^1	
128.8	128.8		$38_1^1 39_0^1$	372.6 − 243.8
143.5	144.8		39_1^2	243.8 − 99.0
151.0	149.2		$38_1^1 39_1^2$	492.8 − 343.6
152.9 sh	152.9		$38_0^1 39_1^0$	251.9 − 99.0
168.6	167.5		39_2^3	364.5 − 197.0
203.5	204.3		$37_0^1 39_1^0$	303.3 − 99.0
243.8	243.8		39_0^2	
243.8	244.9		$36_0^1 39_1^0$	343.9 − 99.0
250.0	249.0		$38_1^1 39_0^2$	492.8 − 243.8
251.9	251.9	250	38_0^1	
264.9	265.5		39_1^3	364.5 − 99.0
270.9 sh	269.2		$38_1^1 39_1^3$	612.8 − 343.6
273.9 sh	273.6		$38_0^1 39_1^1$	372.6 − 99.0
303.3	303.3	298	37_0^1	
343.9	343.9	342	36_0^1	
364.5	364.5		39_0^3	
371.1	369.0		$38_1^1 39_0^3$	612.8 − 243.8
385.3	385.4		39_1^4	484.4 − 99.0
425.4 sh	425.4		$37_0^1 39_0^1$	
465.9	465.9		$36_0^1 39_0^1$	
485.3 sh	484.4 [e]		39_0^4	
487.5	488.2		$36_0^1 39_1^2$	587.2 − 99.0
492.8	492.8		$38_0^1 39_0^2$	
502.2 sh	504.6		39_1^5	603.6 − 99.0
587.2	587.2		$36_0^1 39_0^2$	
603.6	603.6		39_0^5	
607.8	608.5		$36_0^1 39_1^3$	707.5 − 99.0
612.8	612.8		$38_0^1 39_0^3$	
687.0	687.0		36_0^2	
707.5	707.5		$36_0^1 39_0^3$	
721.5	721.5		39_0^6	

[a] Frequencies are relative to the $S_1 \leftarrow S_0$ electronic origin at 26 081.3 cm^{-1}. The uncertainty in the relative frequency is ±0.5 cm^{-1}. [b] Inferred values are based on the energy level diagram in Figure 3. [c] Scaled frequencies calculated using the B3LYP/6-311+G(d,p) level of theory [d] Reference 11. [e] The inferred frequencies for the 39_1^0 and 39_0^4 bands were determined from patterns established by other observed ν_{39} overtones. The inferred values for these two bands were used in the ν_{39} potential energy function determinations. The observed band maxima in these cases led to poorer potential energy fits, most likely because the rotationless band centers (unavailable at the present spectral resolution) are not necessarily coincident with the maxima.

Experimental and Computational Section

The experimental work was carried out at the University of Wisconsin—Eau Claire, using a CRD spectroscopy system that has been described previously in detail.[7] Briefly, the output of a Nd:YAG-pumped pulsed dye laser (approximately 0.5 mJ at 385 nm) was sent through a spatial filter and then into a 1 m CRD cell. The cell was bounded by high-reflectivity mirrors (Los Gatos Research, quoted $R = 0.999\,94$ at 385 nm) with 6 m radii of curvature. The light exiting the cell was detected by a photomultiplier module (Hamamatsu H6780). The photomultiplier signal was sent into the 50 Ω input of a digital oscilloscope (10-bit vertical resolution) and through a 20 MHz internal low-pass filter. The decay traces from typically 16 laser pulses were averaged and then sent to a computer, where a monoexponential rate constant k (along with baseline offset) was determined.

2-Cyclohexen-1-one was purchased from Acros and used without further purification. The deuterated derivative was prepared by combining 2-cyclohexen-1-one (0.1 mol) with D_2O (1.0 mol) and a catalytic amount of D_2SO_4. The mixture was refluxed at 55 °C for 48 h and then extracted with dichloromethane. The solvent was removed by rotary evaporation, and the product was distilled. Analysis by NMR and GC-MS indicated that the product contained approximately 70% 2-cyclohexen-1-one-2,6,6-d_3, with the remainder dideuterated derivatives.

To record the CRD spectra, the liquid sample of 2CHO or 2CHO-d_3 was subjected to several freeze—pump—thaw cycles, and its vapor was admitted to a previously evacuated cell at room temperature. Typically the pressure in the sample cell was maintained at 13 Pa (0.1 Torr). Higher pressures (e.g., close to the 2CHO vapor pressure of 210 Pa) led to CRD signal levels that exceeded the dynamic range of our detection system. Following all of the spectroscopic work on 2CHO-d_0, the sample cell was exposed repeatedly to the 2CHO-d_3 vapor sample. The spectroscopic work on the deuterated sample began after these repeated washings were concluded.

DFT calculations were carried out utilizing the same programs and methods previously described for 2CPO.[14] The geometries for 2CHO and 2-CHO-d_3 were fully optimized using the B3LYP method with the 6-31+G(d,p) and 6-311+G(d,p) basis sets. The S_1 state of 2CHO was generated by selecting appropriate orbital occupancies as an initial guess. Inversion barriers and vibrational frequencies of the molecules in each electronic state were determined from comparison to spectroscopic data. The calculated vibrational frequencies in each electronic state were scaled by 0.9613.[15]

Results and Discussion

Vibronic Analysis. Figures 1 and 2 show the CRD spectra for 2CHO and 2CHO-d_3 in the 26 000—26 700 cm^{-1} region (385 to 375 nm). The vertical axis in Figure 1 indicates fractional photon loss per pass through the cell. The fractional loss was calculated using the expression $(\Delta k)l/c$,[13] where Δk is the observed CRD decay constant with empty-cell value subtracted, l is the length of the cell, and c is the speed of light. The fractional loss, combined with Beer's law, was used determine the molar extinction coefficient (ϵ), which is also plotted in Figure 1.

The vibronic bands in this wavelength region are assigned to the $S_1(n,\pi^*) \leftarrow S_0$ transition of 2CHO. This assignment is based on the observed maximum value of ϵ, consistent with an orbitally forbidden but spin-allowed $\pi^* \leftarrow$ n transition. The similarity in wavelength to the $S_1(n,\pi^*) \leftarrow S_0$ transition of 2CPO (367 nm origin) also supports the electronic assignment of the 2CHO spectrum as $S_1(n,\pi^*) \leftarrow S_0$.

TABLE 2: *CRD Transition Frequencies[a] (cm^{-1}) and Assignments for 2-CHO-d_3

observed	inferred[b]	calculated[c]	assignment	
−300.0	−300.0	−302	37_1^0	
−232.3	−232.3	−224	38_1^0	
−187.6	−187.6		39_2^0	
−94.7	−94.7	−97	39_1^0	
−74.2	−73.2		$38_1^1 39_2^0$	251.9 − 442.2
4.6	4.6		38_1^1	236.9 − 232.3
26.6	26.6		$38_1^1 39_1^1$	350.4 − 323.8
40.0	41.0		39_2^2	122.1 − 197.0
48.1 sh	49.3		$38_0^1 39_2^0$	236.9 − 187.6
114.4	114.4	114	39_0^1	
118.9	118.1		$38_1^1 39_0^1$	350.4 − 232.3
133.1	133.9		39_1^2	228.6 − 94.7
143.0 sh	142.2		$38_0^1 39_1^0$	236.9 − 94.7
154.1 sh	154.2		39_2^3	341.8 − 187.6
201.0	199.9		$37_0^1 39_1^0$	294.6 − 94.7
228.6	228.6		39_0^2	
236.9	236.9	236	38_0^1	
236.9	237.3		$36_0^1 39_1^0$	332.0 − 94.7
247.6	247.1		39_1^3	341.8 − 94.7
256.0	255.7		$38_0^1 39_1^1$	350.4 − 94.7
294.6	294.6	289	37_0^1	
332.0	332.0	332	36_0^1	
341.8	341.8		39_0^3	
350.4	350.4		$38_0^1 39_0^1$	
407.7	407.7		$37_0^1 39_0^1$	
446.2	446.2		$36_0^1 39_0^1$	
466.1	465.3		$36_0^1 39_1^2$	560.0 − 94.7
560.0	560.0		$36_0^1 39_0^2$	
665.2	665.2		36_0^2	
673.4	673.4		$36_0^1 39_0^3$	

[a] Frequencies are relative to the $S_1 \leftarrow S_0$ electronic origin at 26 075.3 cm^{-1}. The uncertainty in the relative frequency is ±0.5 cm^{-1}. [b] Inferred values are based on the energy level diagram in Figure 4. [c] Scaled frequencies calculated using B3LYP/6-311+G(d,p) level of theory.

The band origins (0_0^0) for the two isotopomers are 26 081.3 and 26,075.3 cm^{-1}, respectively.[16] These assignments are based on a series of attached bands observed at approximately 99 cm^{-1} intervals in the d_0 spectrum and extending in the low-frequency direction. An analogous series is observed in the d_3 spectrum at 95 cm^{-1} intervals. These are identified as hot bands and assigned as a progression in ν_{39}'' (ground-state ring inversion), based on the previously determined[10,11] fundamental frequency for this mode in the S_0 state. These hot bands were analyzed in our previous work[11] to determine the inversion potential energy function for the S_0 state.

Extending to the high-frequency direction of the origin is a series of vibronic bands at approximately 122 cm^{-1} intervals in the d_0 spectrum and 114 cm^{-1} in the d_3 spectrum. These series are assigned as progressions in ν_{39}', the excited-state ring inversion mode. Tables 1 and 2 list the positions of these absorption bands for both isotopomers.

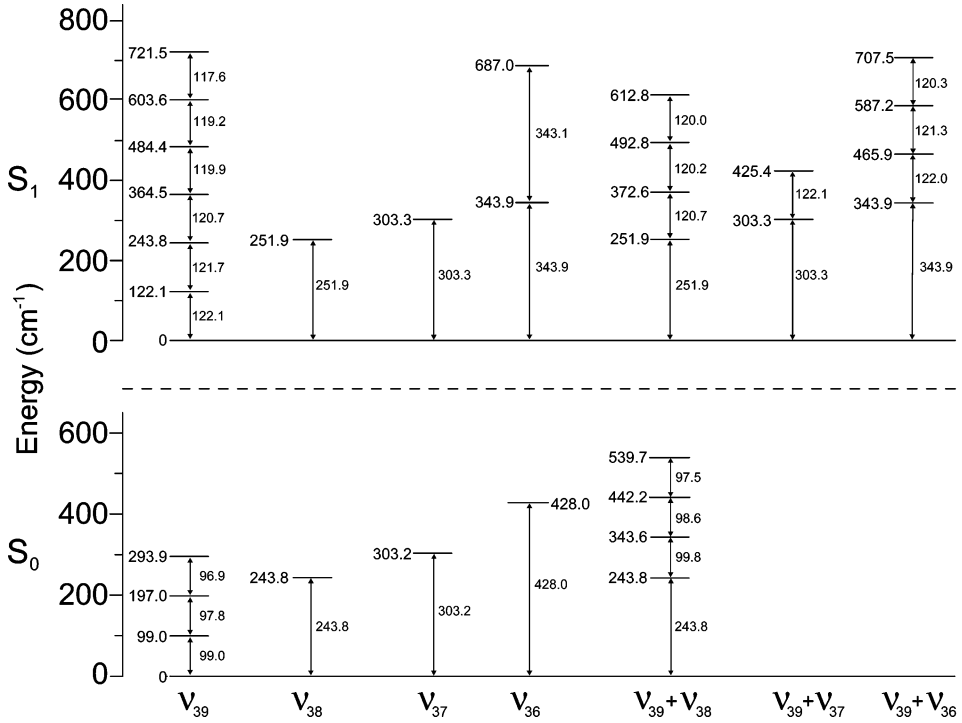

Figure 3. Energy map for 2CHO in its S_0 and $S_1(n,\pi^*)$ electronic states.

Several other low-frequency fundamentals for the S_1 state have been assigned and are listed in Tables 1 and 2. These include ν_{38} (ring bending), ν_{37} (C═C twist), and ν_{36} (carbonyl deformation). These band assignments were made on the basis of similarity to the corresponding fundamental vibrational frequencies in the ground state.[10,11] Frequencies and deuterium shifts predicted from the DFT calculation (discussed below) also support these assignments.

The ν_{38} out-of-plane ring mode has the second-lowest fundamental frequency, 243.0 cm^{-1} in the S_0 state[11] and 251.9 cm^{-1} in the S_1 state for the d_0 isotopomer. At room temperature the $\upsilon_{38}'' = 1$ ground-state level has an appreciable Boltzmann factor (0.3), allowing the 38_1^1 sequence band to appear with relatively large intensity in the CRD spectrum. This band appears at 8.1 cm^{-1} relative to the origin in the d_0 spectrum, consistent with the value of 8.9 cm^{-1} obtained from the $38_0^1 - 38_1^0$ combination difference. In the d_3 spectrum this combination difference is 4.6 cm^{-1} and is reproduced exactly by the 38_1^1 band observed at 4.6 cm^{-1} relative to the origin.

Several of the prominent bands in the CRD spectra, including 38_1^1 and 36_0^1, serve as origins for the 122 (d_0) or 114 cm^{-1} (d_3) progression in the upper-state inversion mode, ν_{39}'. The frequencies of these progressions are listed in Tables 1 and 2.

The spectrum of the deuterated sample contained no resolved features that could be assigned to isotopomers other than 2,6,6-d_3. The most abundant isotopic impurity, according to NMR analysis, is the 6,6-d_2 species. DFT calculations of the vibrational frequencies for these two isotopomers, as well as for the undeuterated molecule, predict isotope shifts most consistent with a d_3 assignment for all of the bands reported in Table 2. Isotopic impurities most likely contribute to broadening of peaks assigned to the d_3 species.

Potential Energy Function for Ring Inversion. Figures 3 and 4 present energy maps for the lower energy quantum states of 2CHO and the d_3 isotopomer. The data for ν_{39} for CHO in the S_0 ground state were previously used[11] to determine its potential energy function. Similar data for the CHO-d_3 will be used in the present work to calculate the quantum states for this isotopomer in the S_0 state. The $S_1(n,\pi^*)$ data in Figures 3 and 4 for both isotopomers will then be used to determine the potential energy functions for the excited state.

To determine the ring-inversion potential energy functions, the kinetic energy (reciprocal reduced mass) expansion must first be calculated. This is based on the structure of the molecule which we calculated by DFT using the B3LYP/6-311+G(d,p) basis set for both the S_0 ground state and the $S_1(n,\pi^*)$ electronic excited state. Figure 5 compares the calculated structures for these two states. As can be seen, the excitation to a π^* antibonding orbital increases the C═C and C═O bond distances as expected. However, the ═C−C(O) bond distance between carbon atoms 1 and 2 decreases from 1.480 to 1.392 Å. Similar changes occur in the 2CPO molecule as a result of $\pi^* \leftarrow$ n excitation.[6,7] In those cases we explained the bond shortening on the basis of the character of the π^* molecular orbitals involved in the conjugation. A qualitative picture of this orbital is shown in Figure 6 for both molecules. As can be seen the C═C and C═O linkages increase in antibonding character whereas the C1−C2 linkage has bonding character in this π^* orbital.

The ring-inversion coordinate S was previously defined[11] and for S_0 involves mostly carbon atoms 6 (next to the C═O group) and 5 moving out of plane. The displacements of carbon atoms 1, 4, 5, and 6 are shown in Table 3 for both S_0 and $S_1(n,\pi^*)$ states based on the DFT calculation. For S_1 an increased out of plane displacement of C4 can be seen as the conjugation is weakened with the $n \rightarrow \pi^*$ transition. For this coordinate the kinetic energy expansion $g_{44}(S)$ was calculated for both 2CHO and 2CHO-d_3 for both S_0 and $S_1(n,\pi^*)$ states, and the coefficients are shown in Table 4. The expansion has the form

$$g_{44}(S) = g_{44}^{(0)} + g_{44}^{(2)}S^2 + g_{44}^{(4)}S^4 + g_{44}^{(6)}S^6 \qquad (1)$$

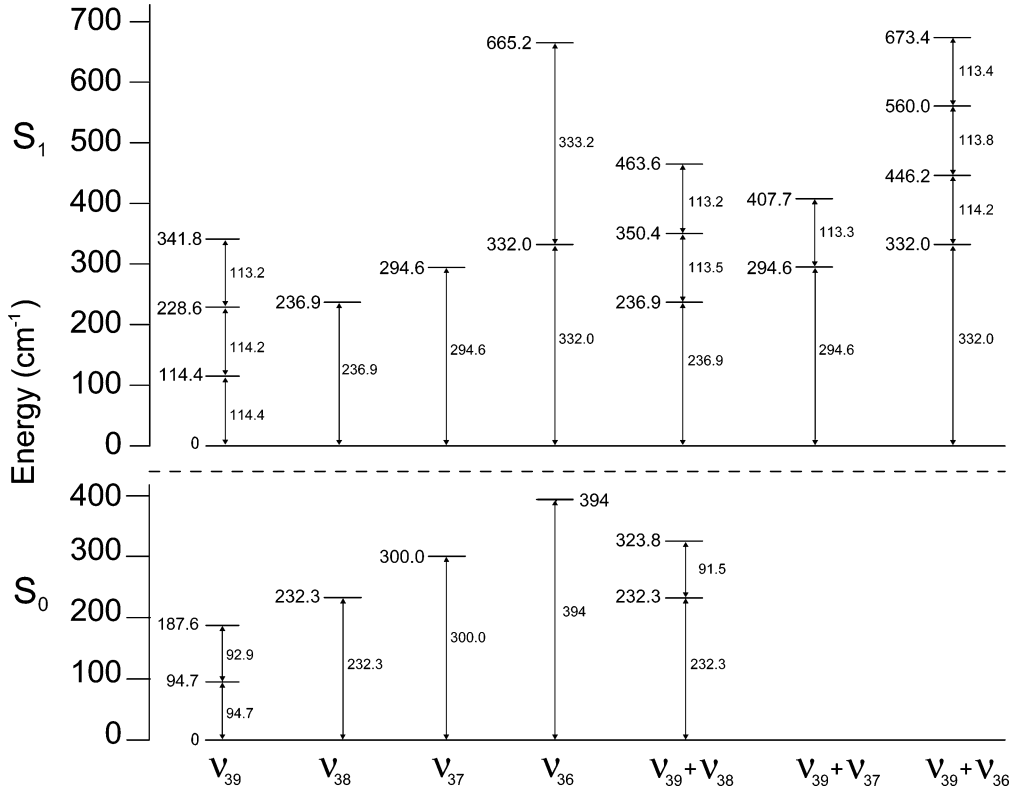

Figure 4. Energy map for 2CHO-d_3 in its S_0 and $S_1(n,\pi^*)$ electronic states.

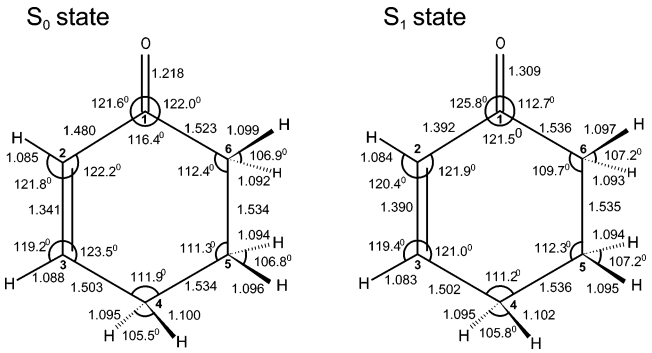

Figure 5. Calculated structures for 2CHO in its S_0 and $S_1(n,\pi^*)$ electronic states.

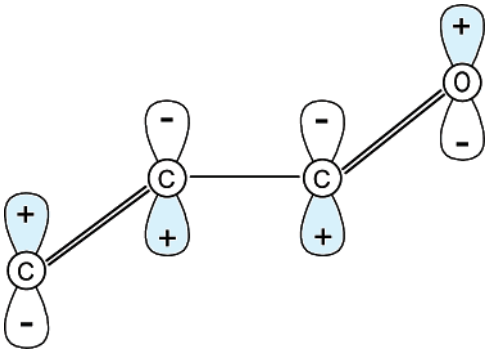

Figure 6. Qualitative picture of the π^* orbital involved in the $\pi^* \leftarrow$ n transition of 2CHO and 2CPO.

where the $g_{44}^{(j)}$ are the coefficients in Table 4. With the availability of the $g_{44}(S)$ expressions, the Hamiltonian

$$\mathcal{H} = -\frac{\hbar^2}{2}\frac{d}{dS}g_{44}(S)\frac{d}{dS} + V(S) \qquad (2)$$

TABLE 3: Calculated[a] Relative Out-of-Plane Displacements (Å) of C1, C4, C5, and C6 Atoms of 2CHO in Its S_0 and $S_1(n,\pi^*)$ States

	S_0	S_1
C1	0.017 523	0.014 228
C4	0.130 933	0.202 797
C5	−0.339 025	−0.340 520
C6	0.269 044	0.200 370

[a] Using B3LYP/6-311+G(d,p) level of theory.

TABLE 4: Calculated Kinetic Energy Coefficients of 2CHO and 2CHO-d_3

		$g_{44}^{(0)}$	$g_{44}^{(2)}$	$g_{44}^{(4)}$	$g_{44}^{(6)}$
S_0	2CHO	0.031 19	−0.047 82	−0.115 30	0.148 96
	2CHO-d_3	0.025 88	−0.022 38	−0.142 63	0.135 38
S_1	2CHO	0.032 11	−0.058 34	−0.130 86	0.226 99
	2CHO-d_3	0.027 75	−0.037 13	−0.144 40	0.167 31

[a] Coefficients are μ^{-1}Å^{-j} for each $g_{44}^{(j)}$.

where

$$V(S) = aS^4 - bS^2 \qquad (3)$$

was used to determine the potential energy parameters a and b which provide the best fit for the experimental data. As reported previously,[11] for 2CHO the potential energy function for the ground state is

$$V(\text{cm}^{-1}) = 7.459 \times 10^2 S^4 - 2.378 \times 10^3 S^2 \qquad (4)$$

and this provides an excellent fit for the S_0 data. The barrier to inversion is 1895 cm^{-1}. This same function should in principle also reproduce the d_3 data when using the correct reduced mass ratio between the d_0 and d_3 isotopomers. This ratio is calculated to be 1.205 (Table 4), but this value results in calculated frequencies which are about 4% too low when eq 4 is used.

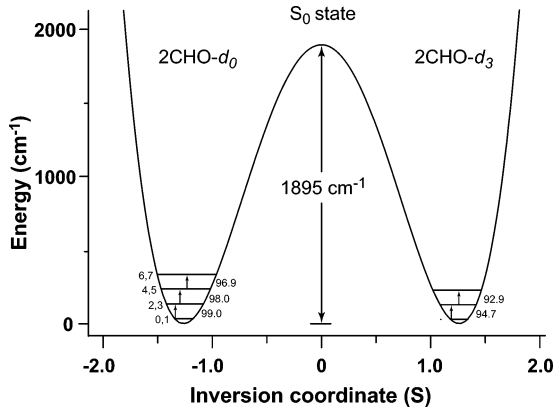

Figure 7. Ring-inversion potential energy function for 2CHO and 2CHO-d_3 in its S_0 state.

TABLE 5: Observed and Calculated Frequencies (cm^{-1}) for the ν_{39} Vibration of 2CHO-d_0 and 2CHO-d_3 in Their S_0 States

	2CHO-d_0		2CHO-d_3	
separation	experimental[a]	calculated	experimental[a]	calculated
0−2	99.0	99.0	94.7	94.7
2−4	98.0	98.0	92.9	93.8
4−6	96.9	96.9		

[a] $V\,(cm^{-1}) = 7.459 \times 10^2 S^4 - 2.378 \times 10^3 S^2$.

TABLE 6: Observed and Calculated Frequencies (cm^{-1}) for the ν_{39} Vibration of 2CHO-d_0 and 2CHO-d_3 in Their $S_1(\pi,\pi^*)$ States

	2CHO-d_0		2CHO-d_3	
separation	experimental[a]	calculated	experimental[a]	calculated
0−2	122.1	122.2	114.4	114.4
2−4	121.7	121.4	114.2	113.7
4−6	120.7	120.5	113.2	113.1
6−8	119.9	119.8		
8−10	119.2	119.1		
10−12	117.9	118.5		

[a] $V\,(cm^{-1}) = 8.586 \times 10^2 S^4 - 3.493 \times 10^3 S^2$.

This is not too surprising since the one-dimensional vibrational model ignores the interactions of the ring inversion with the other 38 vibrations of the molecule. To obtain a satisfactory fit using eq 4 for the d_3 calculation, we adjusted the reduced mass ratio to 1.094. Table 5 compares the observed and calculated energy separation for 2CHO-d_0 and -d_3 based on eq 4 and the adjusted reduced mass ratio. Figure 7 shows this function along with the observed transitions. As discussed previously,[11] the barrier height value is obtained by extrapolation and its accuracy is only ± 300 cm^{-1}.

Using the data in Tables 1 and 2 and Figures 3 and 4, similar calculations were carried out for 2CHO and 2CHO-d_3 for the $S_1(n,\pi^*)$ state. The potential energy function was determined to be

$$V\,(cm^{-1}) = 8.586 \times 10^2 S^4 - 3.493 \times 10^3 S^2 \qquad (5)$$

and the observed and calculated frequencies are shown in Table 6. In this case the calculated reduced mass ratio of 1.157 differs only slightly from the observed value of 1.146, which was used for the computation. If the higher value for the ratio is used, a frequency error of less than 1% would result. Figure 7 shows this function and the observed ν_{39} quantum spacings in the $S_1(n,\pi^*)$ state for both isotopomers. As can be seen for 2CHO, the observed transitions extend to about 800 cm^{-1} above the

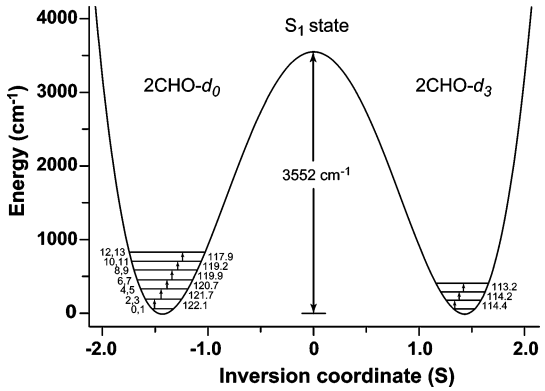

Figure 8. Ring-inversion potential energy function for 2CHO and 2CHO-d_3 in its $S_1(n,\pi^*)$ state.

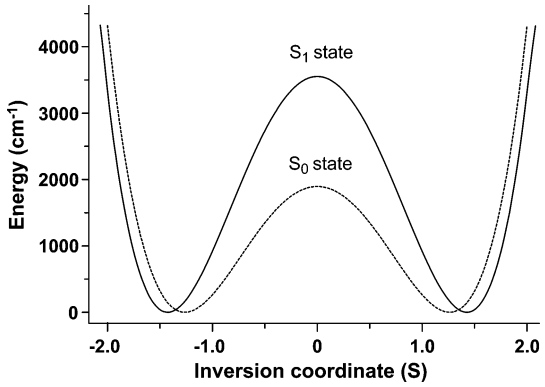

Figure 9. Comparison of the S_0 and $S_1(n,\pi^*)$ ring-inversion potential energy functions.

TABLE 7: Experimental and Calculated Barriers to Planarity (cm^{-1}) of 2CHO in Its S_0 and $S_1(\pi,\pi^*)$ States

	S_0	S_1
experimental	1895	3552
calculated (B3LYP/6-311+G(d,p)	2090	2265

TABLE 8: Observed (CRD) and Calculated (DFT) Frequencies (cm^{-1}) for Low-Frequency Fundamental Vibrations of 2CHO-d_0 and 2CHO-d_3 in Their $S_1(\pi,\pi^*)$ States

	2CHO-d_0		2CHO-d_3	
vibrational mode	CRD[a]	DFT[b]	CRD[a]	DFT[b]
ν_{39}	122.1	120.8	114.4	113.7
ν_{38}	251.9	249.9	236.9	236.1
ν_{37}	303.3	298.4	294.6	289.4
ν_{36}	343.9	341.9	332.0	331.5

[a] Frequency shifts relative to the $S_1 \leftarrow S_0$ band origins in the CRD spectra. [b] B3LYP/6-311+G(d,p) basis set.

energy minimum so the barrier of 3552 cm^{-1} is again obtained by extrapolation. Its uncertainty is estimated to be ± 500 cm^{-1}.

Comparisons with DFT Results. Our DFT calculation using the B3LYP/6-311+G(d,p) basis set predicts a barrier of 2265 cm^{-1} for the $S_1(n,\pi^*)$ state, a value considerably lower than that in Figure 7. The DFT calculation also by definition places the energy minima at $S = \pm 1.0$ Å, while Figure 7 has these at ± 1.4 Å. The conclusion then is that while the DFT calculation predicts a higher barrier for the $S_1(n,\pi^*)$ state than for S_0, it clearly underestimates the barrier and degree of out-of-plane distortion. Most likely, however, our extrapolated experimental barrier is an overestimation. Nonetheless, it is clear that the excited-state value is substantially higher than that in the electronic ground state. Table 7 summarizes both the calculated

and experimental barrier heights for the two electronic states. Figure 9 compares the two experimental potential energy curves.

Although the ν_{39} barrier height from the DFT calculation does not agree quantitatively with the S_1 potential fit, the DFT calculated ν_{39} fundamental frequency (121 cm^{-1}) agrees exceptionally well with that obtained from the CRD spectrum (122.1 cm^{-1}). The agreement is also excellent (typically within 2 cm^{-1} or less) for the other low-frequency fundamentals in the S_1 state. Table 8 shows the calculated DFT and observed values for both isotopomers.

Conclusions

The 2CHO molecule, like many conjugated enones, has nearly zero fluorescence quantum yield following photoexcitation to its $S_1(n,\pi^*)$ state. Therefore this excited state is most amenable to spectroscopic probes based on absorption rather than emission. The high sensitivity of the CRD absorption technique has allowed us to detect the relatively weak absorption spectra corresponding to transitions to the vibronic levels of the $S_1(n,\pi^*)$ state in 2CHO. The data allow the first several quantum states of ν_{39}, the ring-inversion vibration, in this electronic excited state as well as fundamentals of several other low-frequency modes to be determined. The $S_1(n,\pi^*)$ barrier to inversion is found by extrapolation of the potential energy curve to be 3550 $\pm$ 500 cm^{-1} as compared to 1900 $\pm$ 300 cm^{-1} in the S_0 ground state. DFT calculations also predict the barrier in S_1 to be larger, but to a lesser degree. The increase in barrier height likely arises from the decreased conjugation allowing the six-membered ring to distort even further from a planar configuration.

Acknowledgment. J.L. thanks the National Science Foundation (Grant CHE-0131935) and the Robert A. Welch Foundation (Grant A-0396) for financial assistance. Acknowledgment is made by S.D. to the Donors of The Petroleum Research Fund (Grant 42824-B6), administered by the American Chemical Society, for partial support of this research. S.D. also gratefully acknowledges funding from the National Science Foundation (Grant CHE-0517879).

References and Notes

(1) (a) Turro, N. J. *Modern Molecular Photochemistry*; Benjamin/Cummings: Menlo Park, CA, 1978; Chapter 10−12. (b) Schuster, D. I.; Lem, G.; Kaprinidis, N. A. *Chem. Rev.* **1993**, *93*, 23.

(2) (a) García-Expósito, E.; Bearpark, M. J.; Ortuño, R. M.; Robb, M. A.; Branchadell, V. *J. Org. Chem.* **2002**, *67*, 6070. (b) Wilsey, S.; González, L.; Robb, M. A.; Houk, K. N. *J. Am. Chem. Soc.* **2000**, *122*, 5866.

(3) Reguero, M.; Olivucci, M.; Bernardi, F.; Robb, M. A. *J. Org. Chem.* **1997**, *62*, 6897.

(4) Zimmerman, H. E.; Nesterov, E. E. *J. Am. Chem. Soc.* **2003**, *125*, 5422.

(5) Chao, T. H.; Laane, J. *J. Mol. Spectrosc.* **1973**, *48*, 266.

(6) Cheatham, C. M.; Laane, J. *J. Chem. Phys.* **1991**, *94*, 7734.

(7) Pillsbury, N. R.; Choo, J.; Laane, J.; Drucker, S. *J. Phys. Chem. A* **2003**, *107*, 10648.

(8) García-Expósito, E.; Bearpark, M. J.; Ortuño, R. M.; Branchadell, V.; Robb, M. A.; Wilsey, S. *J. Org. Chem.* **2001**, *66*, 8811.

(9) Schuster, D. I.; Dunn, D. A.; Heibel, G. E.; Brown, P. B.; Rao, J. M.; Woning, J.; Bonneau, R. *J. Am. Chem. Soc.* **1991**, *113*, 6245.

(10) Smithson, T. L.; Wieser, H. *J. Chem. Phys.* **1980**, *73*, 2518.

(11) . Gilles, E. J.; Choo, J.; Autrey, D.; Rishard, M.; Drucker, S.; Laane, J. *Can. J. Chem.* **2004**, 82, 867.

(12) Drucker, S. Unpublished observation.

(13) O'Keefe, A.; Deacon, D. A. G. *Rev. Sci. Instrum.* **1988**, *59*, 2544.

(14) Choo, J.; Kim, S.; Drucker, S.; Laane, J. *J. Phys. Chem. A* **2003**, *107*, 10655.

(15) Scott, A. P.; Radom, L. *J. Phys. Chem.* **1996**, *100*, 8782.

(16) In ref 7 we reported the wavenumber of the origin band maximum (2CHO-d_0) as 26 089.1 cm^{-1}. This value is incorrect because we inadvertently neglected to convert calibrated air wavelengths to vacuum. By carrying out the conversion, we obtain a wavenumber value of 26 081.3 cm^{-1} that is used in the present work.